International Journal of Fracture (2005) 135:73–93
DOI 10.1007/s10704-005-3944-5

Crack tip shielding or anti-shielding due to smooth and discontinuous material inhomogeneities

N.K. SIMHA[1,*] F.D. FISCHER[2,3,4], O. KOLEDNIK[3,4], J. PREDAN[5] and G.X. SHAN[6]

[1]*Department of Orthopaedic Surgery, University of Minnesota, MMC 289, 420 Delaware St. SE, Minneapolis, MN 55455, USA*
[2]*Institute of Mechanics, Montanuniversität, Franz-Josef-Strasse 18, A-8700 Leoben, Austria*
[3]*Erich Schmid Institute of Materials Science, Austrian Academy of Sciences, Jahnstrasse 12, A-8700 Leoben, Austria*
[4]*Materials Center Leoben, Franz-Josef-Strasse 13, A-8700 Leoben, Austria*
[5]*Faculty of Mechanical Engineering, University of Maribor, SI-2000 Maribor, Slovenia*
[6]*VOEST Alpine Industrieanlagenbau GmbH&Co, Turmstrasse 44, A-4031 Linz, Austria*
[*]*Author for Correspondence. (E-mail: simha@umn.edu)*

Received 2 February 2005; accepted in revised form 10 October 2005

Abstract. This paper describes a theoretical model and related computational methods for examining the influence of inhomogeneous material properties on the crack driving force in elastic and elastic-plastic materials. Following the configurational forces approach, the crack tip shielding or anti-shielding due to smooth (e.g. graded layer) and discontinuous (e.g. bimaterial interface) distributions in material properties are derived. Computational post-processing methods are described to evaluate these inhomogeneity effects. The utility of the theoretical model and computational methods is demonstrated by examining a bimaterial interface perpendicular to a crack in elastic and elastic-plastic compact tension specimens.

Key words: Composite material, energy release rate, finite element method, fracture toughness, layered material.

1. Introduction

Experiments indicate that bimaterial interfaces have a strong influence on the crack growth rate. For instance, in the experiments of Suresh et al. (1992) and Pippan and Flechsig (2000), the fatigue crack growth rate dropped precipitously as cracks approached the bimaterial interface from the side with the lower yield stress. In contrast, the growth rate seems to increase as the crack approaches from the side with the higher yield stress. Inhomogeneous material properties are inevitable in engineered and biological composites, coatings, surface-treated components and welds on the structural scale and on the microstructural scale due to second-phase particles, inclusions, grain boundaries, twins, etc. Consequently, it is important to understand the influence of the interface on the crack driving force and to develop methods to quantify the inhomogeneity effect in order to tailor the microstructure or the surface treatment to optimize failure properties.

It is convenient to adopt concepts of crack tip shielding or anti-shielding for studying fracture of bodies containing arbitrary distribution of inhomogeneities. The idea is that the inhomogeneities either shield the crack tip from the applied far-field or anti-shield by enhancing the applied far-field stresses. For instance, in the experiments of Suresh et al. (1992); Pippan and Flechsig (2000), a crack tip lying in the softer material is shielded by the bimaterial interface resulting in a slower crack growth rate, whereas the interface enhances (anti-shields) the applied loads for a crack tip lying in the hard material causing an increase in the crack growth rate. In this paper, the shielding or anti-shielding effect of inhomogeneities is quantified by a term C_{inh}, which we call the material inhomogeneity term.

Building on basic works by Eshelby (1970) and others (e.g., Ericksen, 1977 and references in Maugin, 1955), research in the last couple of decades has demonstrated the importance of configurational (or material) forces for studying fracture (Maugin and Trimarco, 1992; Maugin, 1993, 1995; Gurtin, 1955; Gurtin and Podio-Guidugli, 1996). The configurational forces approach has some fundamental advantages for studying fracture: first, in addition to crack growth, it can model diffusion, martensitic and diffusional phase transformations, thin film growth, etc. (Eshelby, 1970; Maugin, 1955; Gurtin, 2000; Kienzler and Herrmann, 2000; Simha, 2000), and hence provides a comprehensive framework for studying the influence of these processes on fracture. Second, based on the configurational balance laws computational errors due to discretization and approximate numerical solution methods can be quantified (Braun, 1997; Mueller et al., 2002). Crack growth corresponds to the movement of the crack tip in the reference configuration and cannot be described as a deformation, since the tip moves from one material point to another. The classical derivation of the crack driving force, J_{tip}, by Rice (1968) considers only the variation of the crack tip in the reference configuration. The configurational forces approach can be viewed as generalizing this to variations of all points in the body. In our opinion, this additional theoretical effort is more than compensated by the advantages listed above. Consequently, we shall follow the configurational forces approach to evaluate the shielding/anti-shielding due to inhomogeneous material properties.

In a recent paper (Simha et al., 2003), we have examined the crack tip shielding/anti-shielding due to a continuous (but arbitrary) distribution of material inhomogeneities. The paper starts with an extensive review of the literature on the influence of inhomogeneities (hence the literature review is brief here). Then, using the configurational forces approach due to Gurtin (1995), the material inhomogeneity term C_{inh}, which quantifies the crack tip shielding/anti-shielding, was derived (first term in Equation (3.4)). The only disadvantage of this expression is that it cannot be directly used with incremental plasticity models, which are preferable since they can account for path-dependent plasticity. For continuous distributions, C_{inh} is related to the derivative of the free energy density at fixed strain; incremental plasticity models are primarily stress based and cannot always be inverted to obtain an explicit dependence on strain. Consequently, a Ramberg-Osgood model equivalent to the incremental plasticity model was used to formally evaluate the inhomogeneity effect in Simha et al. (2003). The predictions, which used the Ramberg-Osgood model, agreed well with independent computational estimates obtained purely from incremental plasticity. Nevertheless, there is no obvious way to prove that this will be true in all cases. Hence it is better if the material inhomogeneity term can be obtained without using strain-based Ramberg-Osgood type

models. The inhomogeneity effect at a sharp interface depends only on the jump of the normal component of the Eshelby tensor at the interface (see Equation (3.4)), and so does not require such models. Since computational studies typically model graded layers as a series of sharp interfaces, the sharp interface results will be more useful.

The rationale for this article is to extend our configurational forces model to discontinuous material inhomogeneities at sharp interfaces and describe computational methods to evaluate the configurational forces as well as the material inhomogeneity term C_{inh}. The material inhomogeneity term is obtained by integrating the configurational body force over the body and the configurational interface force over the interface. Simha et al. (2003) focused on the total effect C_{inh} and did not compute the configurational body force field in a graded interlayer. However, the configurational forces provide a clear visualization of the inhomogeneity effect, so we describe methods to evaluate both the body and interface forces and then discuss their uses. Starting with a compact description of Gurtin's configurational forces approach, the configurational forces in the bulk (2.11), at a sharp interface (2.12) and at the crack tip (2.13) are derived in Section 2. Inhomogeneity effects are examined in Section 3: the material inhomogeneity term C_{inh} is derived, and computational post-processing methods are described. Since recent papers, e.g. Denzer et al. (2003) and Mueller et al. (2004), have described methods to evaluate the configurational body force, we focus on the configurational interface force and the material inhomogeneity term. The utility of the model is demonstrated by evaluating the influence of inhomogeneities in the elastic and elastic-plastic parameters in a bimaterial compact tension specimen (Section 4). Simha et al. (2003) and this paper provide a comprehensive theory and computational tools to examine the influence of continuous and discontinuous material inhomogeneities on the behavior of cracks in elastic and elastic-plastic materials.

2. Balance laws, dissipation inequality, *J*-integral

The configurational forces approach of Gurtin follows engineering methods based on free body diagrams (Gurtin, 1995, 2000); essentially an arbitrary region in a body is considered, the influence of the remainder of the body is replaced by tractions on the boundary of the region and the sum of all forces acting on the body is set to zero (statics). The primary new ingredient is that the approach considers two force systems. One is due to the usual Newtonian forces, which are the thermodynamic forces conjugate to deformation. A separate system of forces that are conjugate to motions in the reference, called the configurational forces, is introduced. Crack growth may require energy due to deformation but the growth cannot be described as a deformation, since the crack tip moves from one material point to another during crack growth. Instead growth corresponds to a motion of the tip in the reference configuration. Similarly, grain boundary coarsening, phase boundary and dislocation movements need to be described as motions in the reference (see e.g., Gurtin, 1995; Maugin, 1995; Simha and Bhattacharya, 1998). Balance laws are obtained for the Newtonian forces by using a free-body diagram in the current configuration, whereas the balance laws for the configurational forces are obtained by a free-body diagram in the reference configuration. These balance laws and certain invariance requirements for the second law of thermodynamics provide all the relations relevant for studying cracks in inhomogeneous bodies.

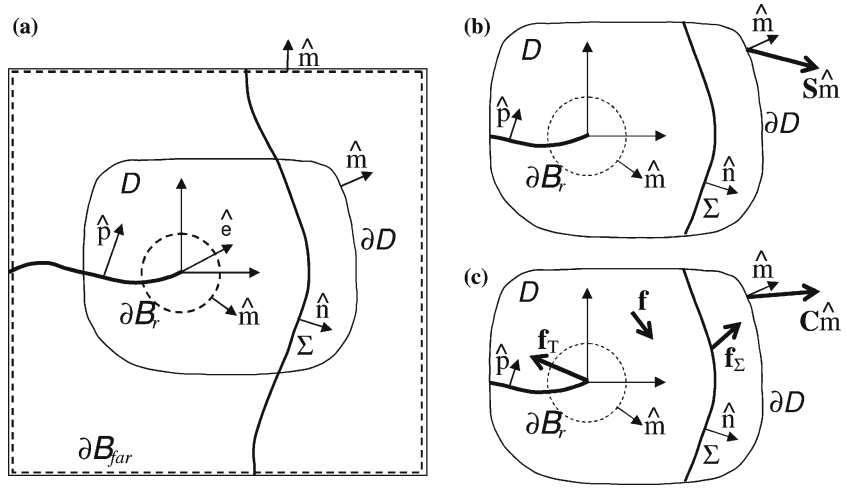

Figure 1. (a) A two-dimensional body $\mathcal{B}$ containing a crack and a sharp interface Σ in the reference configuration. The (unit) normal to the interface is $\hat{\mathbf{n}}$ and to the crack is $\hat{\mathbf{p}}$; the direction of crack growth is $\hat{\mathbf{e}}$; (b) deformational forces on subregion $\mathcal{D}$ and (c) Configurational forces acting on subregion $\mathcal{D}$.

Consider the simple setting of a two-dimensional body $\mathcal{B}$ in the reference configuration with no heat conduction and no inertia. The crack is treated as a curve with a unit normal $\hat{\mathbf{p}}$ and the interface is also a curve with unit normal $\hat{\mathbf{n}}$ (see Figure 1). No assumptions are made for either the (continuous) distribution of the inhomogeneities or the constitutive nature of the body. The deformational force system consists of only the engineering (Piola-Kirchhoff) stress $\mathbf{S}$ in the reference configuration. Strictly speaking, the balance of deformational force should be written in terms of the Cauchy stress in the current configuration. However, the transformations between the Cauchy and Piola-Kirchoff stresses allow for equivalent statements in the reference configuration, so for brevity we do all calculations in the reference. For an arbitrary region $\mathcal{D}$ containing the crack tip and intersecting with the sharp interface Σ, the only deformational force is the contact force $\mathbf{S}\hat{\mathbf{m}}$ on the boundary $\partial\mathcal{D}$ where $\hat{\mathbf{m}}$ denotes the unit normal to $\partial\mathcal{D}$ (Figure 1b). Consequently, the balance of the deformational forces is

$$\int_{\partial\mathcal{D}} \mathbf{S}\hat{\mathbf{m}}\,\mathrm{d}l = \mathbf{0} \quad \text{for every region } \mathcal{D}.$$

The stresses can be singular at the crack tip, and in addition, a sharp interface is present, so the standard divergence theorem has been modified in Appendix A. Then, since the force balance is valid for every region $\mathcal{D}$, we apply the modified divergence theorem (A2) and obtain

$$\nabla\cdot\mathbf{S} = \mathbf{0} \quad \text{at each point in the body,} \tag{2.1}$$

$$[[\mathbf{S}]]\,\hat{\mathbf{n}} = \mathbf{0} \quad \text{at the sharp interface,} \tag{2.2}$$

$$\mathbf{S}\hat{\mathbf{p}} = \mathbf{0} \quad \text{on the two crack faces,} \tag{2.3}$$

$$\lim_{r\to 0}\int_{\partial\mathcal{B}_r} \mathbf{S}\hat{\mathbf{m}}\,\mathrm{d}l = \mathbf{0} \quad \text{at the crack tip} \tag{2.4}$$

where ∇ is the Lagrangian gradient operator and $[[\mathbf{b}]]$ denotes the jump in $\mathbf{b}$ at the interface Σ. Equation (2.1) is the familiar equilibrium equation of continuum mechanics, Equation (2.2) ensures traction continuity at the sharp interface, Equation (2.3) is trivially satisfied since the crack faces are traction free, and Equation (2.4) imposes restrictions on the singular nature of the stress field near the crack tip. Equations (2.1, 2.3 and 2.4) correspond to the quasistatic crack problem, and are satisfied by the K-field of LEFM, for instance.

For the configurational force system, a stress $\mathbf{C}$ and a body force $\mathbf{f}$ are taken for the bulk of the body, only a force $\mathbf{f}_\Sigma$ is taken for the interface, while the crack tip can support a configurational force $\mathbf{f}_\mathrm{T}$. The following configurational forces act on an arbitrary region $\mathcal{D}$ containing the crack tip and intersecting with the sharp interface Σ (Figure 1c): body force $\mathbf{f}$ in the area $\mathcal{D}$, contact force $\mathbf{C}\hat{\mathbf{m}}$ on $\partial\mathcal{D}$, interface force $\mathbf{f}_\Sigma$ on the interface Σ, and the point force $\mathbf{f}_\mathrm{T}$ at the crack tip. Thus the balance of configurational forces is

$$\int_{\mathcal{D}} \mathbf{f}\,\mathrm{d}A + \int_{\Sigma\cap\mathcal{D}} \mathbf{f}_\Sigma\,\mathrm{d}l + \int_{\partial\mathcal{D}} \mathbf{C}\hat{\mathbf{m}}\,\mathrm{d}l + \mathbf{f}_\mathrm{T} = \mathbf{0} \quad \text{for every region } \mathcal{D}.$$

Again, since this is valid for each region $\mathcal{D}$, we apply the divergence theorem (A2) and obtain

$$\nabla\cdot\mathbf{C} + \mathbf{f} = \mathbf{0} \quad \text{at each point in the body,} \tag{2.5}$$

$$[[\mathbf{C}]]\hat{\mathbf{n}} + \mathbf{f}_\Sigma = \mathbf{0} \quad \text{at the sharp interface,} \tag{2.6}$$

$$\mathbf{C}\hat{\mathbf{p}} = \mathbf{0} \quad \text{on the two crack faces,} \tag{2.7}$$

$$\lim_{r\to 0}\int_{\partial\mathcal{B}_r} \mathbf{C}\hat{\mathbf{m}}\,\mathrm{d}l + \mathbf{f}_\mathrm{T} = \mathbf{0} \quad \text{at the crack tip.} \tag{2.8}$$

The utility of these additional equations are elucidated in the discussion. Briefly, the configurational forces $\mathbf{f}$ and $\mathbf{f}_\Sigma$ will help evaluate the effect of inhomogeneities, while $(-\mathbf{f}_\mathrm{T})$ is the thermodynamic driving force for crack growth. Below, we will see that the configurational stress $\mathbf{C}$ is related to the equilibrium stress, deformation and strain energy (2.9); then, the above equations will define the configurational forces.

The second law of thermodynamics that is valid for this mechanical setting is the Clausius-Duhem inequality, which requires that the dissipation be non-negative for every subregion $\mathcal{D}$ of the body $\mathcal{B}$; the dissipation is the difference between the rate of working and the rate of change of energy. Applying certain invariance requirements on the Clausius-Duhem inequality results in the following: first, the bulk configurational stress is (Gurtin 1995)

$$\mathbf{C} = \phi\mathbf{I} - \mathbf{F}^\mathrm{T}\mathbf{S}, \tag{2.9}$$

where ϕ is the (Helmholtz) potential or the stored energy density and $\mathbf{F}$ is the deformation gradient. Thus $\mathbf{C}$ is the Eshelby's energy-momentum tensor (Eshelby, 1970), which we shall henceforth call the Eshelby tensor. Second, the total dissipation Γ in the body is (Gurtin and Podio-Guidugli, 1996)

$$\Gamma(\mathcal{B}) = \int_{\mathcal{B}} \left(\mathbf{S}\cdot\dot{\mathbf{F}} - \dot{\phi}\right)\mathrm{d}A \; + (-\mathbf{f}_\mathrm{T})\cdot\mathbf{v}_\mathrm{T} \geqslant 0\,, \tag{2.10}$$

where $\dot{\mathbf{F}}$ denotes the Lagrangian time derivative of $\mathbf{F}$, $\mathbf{v}_T$ is the crack tip velocity (in the reference configuration). Equations (2.9) and (2.10) are derived in Simha et al. (2003) (sharp interfaces are not considered there, but the bimaterial interface does not move and hence those derivations are still valid).

Now that the configurational stress is known, the force balances (2.5)–(2.8) are used to write the configurational forces as

$$\mathbf{f} = -\nabla \cdot \left(\phi \mathbf{I} - \mathbf{F}^T \mathbf{S}\right), \tag{2.11}$$

$$\mathbf{f}_\Sigma = -\left[\left[\phi \mathbf{I} - \mathbf{F}^T \mathbf{S}\right]\right] \hat{\mathbf{n}} = -\left([[\phi]]\mathbf{I} - [[\mathbf{F}^T]]\langle \mathbf{S} \rangle\right) \hat{\mathbf{n}}, \tag{2.12}$$

$$\mathbf{f}_T = -\lim_{r \to 0} \int_{\partial \mathcal{B}_r} \left(\phi \mathbf{I} - \mathbf{F}^T \mathbf{S}\right) \hat{\mathbf{m}} \, \mathrm{d}l, \tag{2.13}$$

where $\langle b \rangle$ denotes the average of the quantity b at the interface Σ; the traction continuity (2.2) and the identity

$$[[\mathbf{F}^T \mathbf{S}]] = [[\mathbf{F}]]^T \langle \mathbf{S} \rangle + \langle \mathbf{F}^T \rangle [[\mathbf{S}]]$$

have been used to simplify $\mathbf{f}_\Sigma$. Thus the configurational body force $\mathbf{f}$ is the negative of the (Lagrangian) divergence of the Eshelby tensor; the configurational interface force $\mathbf{f}_\Sigma$ is the negative of the normal component of the jump in the Eshelby tensor, whereas the configurational force at the crack tip $\mathbf{f}_T$ is the negative of the limiting value of the contour integral of the contact force ($\mathbf{C}\hat{\mathbf{m}}$) due to the Eshelby tensor as the contour radius vanishes.

Localizing (2.10), we obtain the dissipation at each point in the body as (Simha et al., 2003)

$$\Gamma_{\text{bulk}} = \mathbf{S} \cdot \dot{\mathbf{F}} - \dot{\phi} \geqslant 0, \tag{2.14}$$

whereas the dissipation due to the crack tip growing with a velocity $\mathbf{v}_T$ is

$$\Gamma_{\text{tip}} = (-\mathbf{f}_T) \cdot \mathbf{v}_T \geqslant 0. \tag{2.15}$$

Notice that (2.14) accounts for dissipation (including plastic) in the bulk. For the crack tip (2.15) is the second law of thermodynamics; hence, by following classical reasoning, we identify $(-\mathbf{f}_T)$ as the crack driving force, since it is the force term conjugate to the crack tip velocity. In fracture mechanics the energy dissipated per unit crack extension is commonly used, and it is equal to

$$J_{\text{tip}} \equiv \hat{\mathbf{e}} \cdot (-\mathbf{f}_T) = \hat{\mathbf{e}} \cdot \lim_{r \to 0} \int_{\partial \mathcal{B}_r} \left(\phi \mathbf{I} - \mathbf{F}^T \mathbf{S}\right) \hat{\mathbf{m}} \, \mathrm{d}l \geqslant 0, \tag{2.16}$$

where the unit vector $\hat{\mathbf{e}} = \mathbf{v}_T / |\mathbf{v}_T|$ lies along the direction of crack growth. This is Rice's J-integral written in direct notation for the finite strain setting. It is obtained as the projection of the vector driving force $(-\mathbf{f}_T)$ along the direction of crack growth $\hat{\mathbf{e}}$, and is hence a scalar crack tip driving force.

Finally, the relation between the crack tip and far field J-integrals is obtained using the balance of configurational forces for a region $\mathcal{D}$ that does not contain the crack tip. Instead, it is bounded by two contours $\partial \mathcal{B}_1$, $\partial \mathcal{B}_2$ and the crack faces ($\partial \mathcal{B}_1$

is closer to crack tip than $\partial\mathcal{B}_2$ and normals point away from the tip). This force balance is

$$\int_{\partial\mathcal{B}_2} \mathbf{C}\hat{\mathbf{m}}\,\mathrm{d}l - \int_{\partial\mathcal{B}_1} \mathbf{C}\hat{\mathbf{m}}\,\mathrm{d}l + \int_{\mathcal{D}} \mathbf{f}\,\mathrm{d}A \; + \int_{\Sigma\cap\mathcal{D}} \mathbf{f}_\Sigma\,\mathrm{d}l = 0$$

by taking the scalar product of this equation with $\hat{\mathbf{e}}$, setting $\partial\mathcal{B}_1$ to be the crack tip contour $\partial\mathcal{B}_r$, $\partial\mathcal{B}_2$ to be $\partial\mathcal{B}_{\text{far}}$ (Figure 1), and taking the limit as the tip contour vanishes, we obtain

$$J_{\text{tip}} - J_{\text{far}} = \hat{\mathbf{e}}\cdot\int_{\mathcal{B}} \mathbf{f}\,\mathrm{d}A + \hat{\mathbf{e}}\cdot\int_{\Sigma} \mathbf{f}_\Sigma\,\mathrm{d}l, \tag{2.17}$$

where $\mathcal{B}$ is the entire body but does not contain the crack tip. Notice that the above relation has been derived without using any specific form for the stored energy density ϕ. Consequently it is valid even for elastic-plastic and other dissipative materials.

In this section we have followed Gurtin's configurational forces approach to identify the Eshelby tensor (2.9), the configurational body forces (2.11)–(2.13), and relate the crack tip and far-field integrals (2.17). Alternate approaches for obtaining these equations can be found in Maugin (1995) and Kienzler and Herrmann (2000) for instance. The expression for the interface configurational force was first derived in the context of phase boundaries by Truskinovsky (1982) and Abeyaratne and Knowles (1990).

3. Effects of sharp and continuous inhomogeneities

The relation (2.17) provides the basis for examining the effects of inhomogeneous material properties. We first rewrite the configurational interface force $\mathbf{f}_\Sigma$, which appears in the second integral in (2.17) in a more convenient form. The force $\mathbf{f}_\Sigma$ is still given by (2.12) and its component along the crack growth direction is

$$\hat{\mathbf{e}}\cdot\mathbf{f}_\Sigma = -\hat{\mathbf{e}}\cdot\left([[\phi]]\mathbf{I} - [[\mathbf{F}^{\mathrm{T}}]]\langle\mathbf{S}\rangle\right)\hat{\mathbf{n}}.$$

This can be written in a computationally more efficient form by using the Hadamard condition

$$[[\mathbf{F}]] = [[\mathbf{F}]]\hat{\mathbf{n}}\otimes\hat{\mathbf{n}}, \tag{3.1}$$

which is required since continuous deformations and discontinuous material properties can result in discontinuous deformation gradients at a bimaterial interface. First, note $[[\mathbf{F}]]\hat{\mathbf{e}} = (\hat{\mathbf{n}}\cdot\hat{\mathbf{e}})[[\mathbf{F}]]\hat{\mathbf{n}}$, then

$$\hat{\mathbf{e}}\cdot[[\mathbf{F}^{\mathrm{T}}]]\langle\mathbf{S}\rangle\hat{\mathbf{n}} = [[\mathbf{F}]]\hat{\mathbf{e}}\cdot\langle\mathbf{S}\rangle\hat{\mathbf{n}} = (\hat{\mathbf{n}}\cdot\hat{\mathbf{e}})[[\mathbf{F}]]\hat{\mathbf{n}}\cdot\langle\mathbf{S}\rangle\hat{\mathbf{n}}\,.$$

Next, using the trace operator we see that

$$[[\mathbf{F}]]\hat{\mathbf{n}}\cdot\langle\mathbf{S}\rangle\hat{\mathbf{n}} \;= tr\left([[\mathbf{F}]]\hat{\mathbf{n}}\otimes\langle\mathbf{S}\rangle\hat{\mathbf{n}}\right).$$

For arbitrary vectors $\mathbf{a}$, $\mathbf{b}$ and an arbitrary tensor $\mathbf{B}$, we have the identity $(\mathbf{a}\otimes\mathbf{B}\mathbf{b}) = (\mathbf{a}\otimes\mathbf{b})\mathbf{B}^{\mathrm{T}}$, which implies that

$$\begin{aligned}[[\mathbf{F}]]\hat{\mathbf{n}}\cdot\langle\mathbf{S}\rangle\hat{\mathbf{n}} &= tr\left(\left\{[[\mathbf{F}]]\hat{\mathbf{n}}\otimes\hat{\mathbf{n}}\right\}\langle\mathbf{S}^{\mathrm{T}}\rangle\right)\\ &= tr\left([[\mathbf{F}]]\langle\mathbf{S}^{\mathrm{T}}\rangle\right) = \langle\mathbf{S}\rangle\cdot[[\mathbf{F}]],\end{aligned}$$

where we once again use the Hadamard condition (3.1). These steps can be easily derived using Cartesian components as

$$[[\mathbf{F}]]\hat{\mathbf{n}}\cdot\langle\mathbf{S}\rangle\hat{\mathbf{n}} = [[F_{ij}]]\hat{n}_j\langle S_{ik}\rangle\hat{n}_k = [[F_{ij}]]\hat{n}_j\hat{n}_k\langle S_{ik}\rangle = [[F_{ik}]]\langle S_{ik}\rangle = \langle\mathbf{S}\rangle\cdot[[\mathbf{F}]].$$

Thus, the configurational interface force component along the crack growth direction is

$$\hat{\mathbf{e}}\cdot\mathbf{f}_\Sigma = -\hat{\mathbf{e}}\cdot\left([[\phi]]\mathbf{I} - [[\mathbf{F}^{\mathrm{T}}]]\langle\mathbf{S}\rangle\right)\hat{\mathbf{n}} = -\left([[\phi]] - \langle\mathbf{S}\rangle\cdot[[\mathbf{F}]]\right)(\hat{\mathbf{n}}\cdot\hat{\mathbf{e}})\,. \tag{3.2}$$

It is easier to compute the second form, especially when the interface is flat. Note that we did not make specific constitutive assumptions for ϕ; it is merely the stored energy density.

In contrast, specific constitutive relations are necessary and a model for inhomogeneities is needed to obtain simplified forms for the configurational body force $\mathbf{f}$, which appears in the first integral in (2.17). To model inhomogeneities a simple choice is to make the free energy ϕ depend on the reference coordinate $\mathbf{x}\in\mathcal{B}$. Next, we consider hyperelastic materials and take $\phi = \phi(\mathbf{F},\mathbf{x})$. Then, it can be shown that (2.11) reduces to (Simha et al., 2003)

$$\mathbf{f} = -\nabla\cdot(\phi\mathbf{I} - \mathbf{F}^{\mathrm{T}}\mathbf{S}) = -\nabla_{\mathbf{x}}\phi(\mathbf{F},\mathbf{x}). \tag{3.3}$$

Thus, the configurational body force is equal to the Lagrangian gradient of the stored energy density (explicit derivative taken at fixed deformation gradient). In this context, elastic-plastic materials can be treated using deformational plasticity which is appropriate for proportional loading conditions. Incremental plasticity can be modeled by using $\phi = \phi(\mathbf{F}^{\mathrm{e}},\mathbf{x})$ where $\mathbf{F}^{\mathrm{e}}$ denotes the elastic portion of the deformation gradient (Maugin, 1995); we are pursuing this currently and results will be reported elsewhere.

We formally define the material inhomogeneity term as

$$C_{\mathrm{inh}} \equiv -\hat{\mathbf{e}}\cdot\left(\int_{\mathcal{B}}\nabla_{\mathbf{x}}\phi(\mathbf{F},\mathbf{x})\,\mathrm{d}A + \int_\Sigma\left([[\phi]]\mathbf{I} - [[\mathbf{F}^{\mathrm{T}}]]\langle\mathbf{S}\rangle\right)\hat{\mathbf{n}}\,\mathrm{d}l\right) \tag{3.4}$$

$$= -\hat{\mathbf{e}}\cdot\int_{\mathcal{B}}\nabla_{\mathbf{x}}\phi(\mathbf{F},\mathbf{x})\,\mathrm{d}A - \int_\Sigma\left([[\phi]] - \langle\mathbf{S}\rangle\cdot[[\mathbf{F}]]\right)(\hat{\mathbf{n}}\cdot\hat{\mathbf{e}})\,\mathrm{d}l\,. \tag{3.5}$$

The integrals on the right-hand side of (3.4) form a vector representing the total material force due to inhomogeneities in the cracked body $\mathcal{B}$; the first integral is due to a smooth distribution of inhomogeneities, while the second is due to the sharp interface. The scalar quantity C_{inh} is the projection of this vector in the direction of the crack growth $\hat{\mathbf{e}}$. This is the additional term that quantifies the crack tip shielding or anti-shielding and originates from material inhomogeneity in the direction of crack growth. The contribution of each material point in the bulk is $(\mathbf{f}\cdot\hat{\mathbf{e}})$ and of each point on the interface is $(\mathbf{f}_\Sigma\cdot\hat{\mathbf{e}})$. Finally, from (2.17), the effect of inhomogeneities on the crack tip driving force is

$$J_{\mathrm{tip}} = J_{\mathrm{far}} + C_{\mathrm{inh}}\,. \tag{3.6}$$

The field equations relevant for a crack in an inhomogeneous body are (i) the equilibrium conditions: bulk equilibrium (2.1); traction-free crack faces (2.3), traction

continuity (2.2) and deformation compatibility (3.1) at any sharp interfaces and relevant far-field boundary conditions; (ii) the driving force at the crack tip (2.16); (iii) the configurational body force (3.3), the configurational interface force (2.12) and the material inhomogeneity term (3.4) or (3.5); and (iv) the effect of inhomogeneities on the crack tip driving force (3.6).

As numerous applications work with infinitesimal strains, we will now rewrite relevant equations for the small strain setting. Denoting the Cauchy stress by $\boldsymbol{\sigma}$, the displacement by $\mathbf{u}$ and the linear strain by $\boldsymbol{\epsilon} = (\nabla\mathbf{u} + \nabla\mathbf{u}^{\mathrm{T}})/2$, the required equations are

$$\nabla \cdot \boldsymbol{\sigma} = \mathbf{0} \qquad \text{in the cracked body,} \tag{3.7}$$

$$[[\boldsymbol{\sigma}]]\hat{\mathbf{n}} = \mathbf{0} \quad \text{and} \quad [[\nabla\mathbf{u}]] = [[\nabla\mathbf{u}]]\hat{\mathbf{n}} \otimes \hat{\mathbf{n}} \qquad \text{at any sharp interfaces,} \tag{3.8}$$

$$\boldsymbol{\sigma}\,\hat{\mathbf{p}} = \mathbf{0} \qquad \text{on the crack faces,} \tag{3.9}$$

$$J_{\mathrm{tip}} = \hat{\mathbf{e}} \cdot \lim_{r \to 0} \int_{\partial \mathcal{B}_r} (\phi \mathbf{I} - \nabla\mathbf{u}^{\mathrm{T}}\boldsymbol{\sigma})\,\hat{\mathbf{m}}\,\mathrm{d}l\,, \tag{3.10}$$

$$\mathbf{f} = -\nabla_{\mathbf{x}}\phi(\boldsymbol{\epsilon}, \mathbf{x}), \tag{3.11}$$

$$\mathbf{f}_{\Sigma} = -\left([[\phi]]\mathbf{I} - [[\nabla\mathbf{u}^{\mathrm{T}}]]\langle\boldsymbol{\sigma}\rangle\right)\hat{\mathbf{n}}\,, \quad \mathbf{e}\cdot\mathbf{f}_{\Sigma} = -\left([[\phi]] - \langle\boldsymbol{\sigma}\rangle\cdot[[\boldsymbol{\epsilon}]]\right)(\mathbf{e}\cdot\hat{\mathbf{n}}), \tag{3.12}$$

$$\begin{aligned} C_{\mathrm{inh}} &= -\hat{\mathbf{e}}\cdot\left(\int_{\mathcal{B}} \nabla_{\mathbf{x}}\phi(\boldsymbol{\epsilon}, \mathbf{x})\,\mathrm{d}A + \int_{\Sigma}\left([[\phi]]\mathbf{I} - [[\nabla\mathbf{u}]]^{\mathrm{T}}\langle\boldsymbol{\sigma}\rangle\right)\hat{\mathbf{n}}\,\mathrm{d}l\right) \\ &= -\hat{\mathbf{e}}\cdot\int_{\mathcal{B}} \nabla_{\mathbf{x}}\phi(\boldsymbol{\epsilon}, \mathbf{x})\,\mathrm{d}A - \int_{\Sigma}\left([[\phi]] - \langle\boldsymbol{\sigma}\rangle\cdot[[\boldsymbol{\epsilon}]]\right)(\hat{\mathbf{n}}\cdot\hat{\mathbf{e}})\,\mathrm{d}l, \end{aligned} \tag{3.13}$$

$$J_{\mathrm{tip}} = J_{\mathrm{far}} + C_{\mathrm{inh}}\,. \tag{3.14}$$

Equations (3.7)–(3.9) are the standard equilibrium equations and (3.10) is the standard J-integral written in direct notation. The configurational forces are given by (3.11) and (3.12), while the material inhomogeneity term is obtained from (3.13) and inhomogeneity effects on the crack driving force is given by (3.14). Finally, with elastic applications in mind, we have obtained reduced expressions for $\mathbf{f}$, $\mathbf{f}_{\Sigma}$, and C_{inh} in terms of the linear elastic moduli in Appendix B.

Notice that the configurational forces and the material inhomogeneity term essentially need the equilibrium stress, strain and displacement fields. The stored energy density, stress and strain (or deformation gradient) can be determined by a standard numerical calculation. Consequently, there is no need to solve a separate numerical problem to determine the configurational forces. Instead, the configurational forces $\mathbf{f}$ and $\mathbf{f}_{\Sigma}$ as well as the material inhomogeneity effect C_{inh} can be obtained by post-processing.

Recent studies provide methods for evaluating the configurational body force (Mueller et al., 2002; Denzer et al., 2003). Mueller et al. (2004) describe a post-processor based on the same discretization and shape functions used for the stress analysis. In the context of inhomogeneous materials with smooth variations, Simha et al. (2003) obtained the configurational body force by explicitly calculating the gradient of the strain energy density (3.3); then the inhomogeneity effect was calculated by integrating over the entire cracked body. Since these methods are already available in the literature, the rest of this section will only discuss a post-processor for evaluating $\mathbf{f}_{\Sigma}$ and the corresponding inhomogeneity effect.

The configurational interface force $\mathbf{f}_{\Sigma}$ is evaluated as follows. At each node on the interface the limiting values of the strain energy density ϕ^{+}, Cauchy stress σ_{ij}^{+} and

displacement gradient $u^+_{i,j}$ are obtained by extrapolating from the integration points in the element on the + side of the interface; similarly ϕ^-, σ^-_{ij}, and $u^-_{i,j}$ are obtained from the element on the − side (interface normal $\hat{\mathbf{n}}$ points from the − to the + side). Then, at each node, the Cartesian components of the configurational interface force are calculated as

$$(\mathbf{f}_\Sigma)_i = -\left([\phi^+ - \phi^-]\delta_{ik} - [u^+_{j,i} - u^-_{j,i}]\frac{\sigma^+_{jk} + \sigma^-_{jk}}{2} \right) n_k, \tag{3.15}$$

where δ_{ik} is the Kronecker delta and repeated indices are to be summed. Alternately, the component along the direction of crack growth can be calculated using

$$\hat{\mathbf{e}} \cdot \mathbf{f}_\Sigma = -\left([\phi^+ - \phi^-] - [u^+_{j,i} - u^-_{j,i}]\frac{\sigma^+_{ji} + \sigma^-_{ji}}{2} \right) (e_k n_k). \tag{3.16}$$

The contribution of the interface to the inhomogeneity term C_{inh} is then obtained by using the trapezoid formula to integrate the nodal values of $\hat{\mathbf{e}} \cdot \mathbf{f}_\Sigma$ from (3.16).

4. Influence of a sharp bimaterial interface

In Simha et al. (2003) the influence of a graded interlayer was explained by evaluating C_{inh}; systematic case studies considered inhomogeneous elastic and elastic-plastic properties. Here, we focus on discontinuous property changes and demonstrate the utility of the configurational interface force $\mathbf{f}_\Sigma$ in studying inhomogeneity effects. A compact tension (CT) specimen (width 50 mm, height h=30 mm) containing a sharp bimaterial interface will be considered (see Figure 2). The CT specimen has a crack

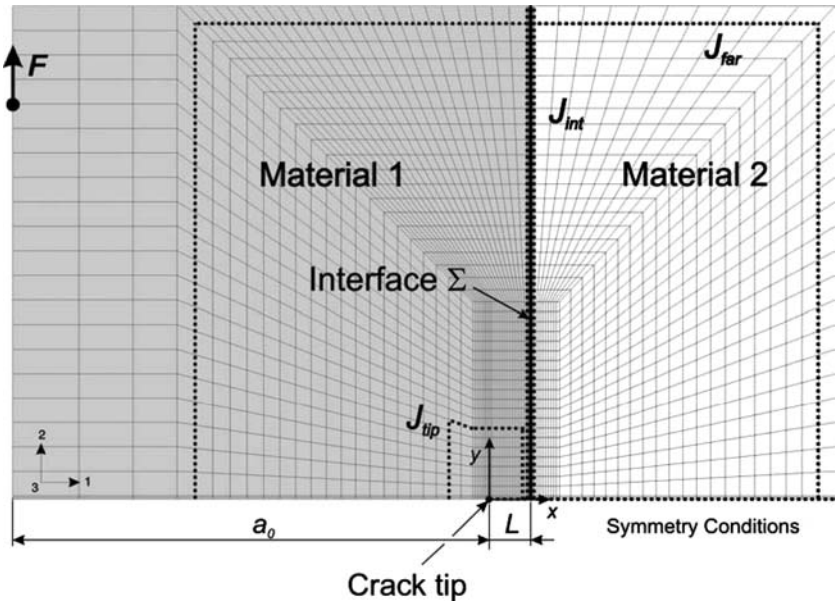

Figure 2. The finite-element mesh of the CT specimen with a bimaterial interface perpendicular to the crack. The crack length $a_o = 29$ mm, while the distance between the crack tip and the interface is $L = 0.6$ mm. Contours like the ones used for evaluating the J-integrals are shown.

of length 29 mm and the interface is at a distance of $L = 0.60$ mm in front of and perpendicular to the crack. The finite-element package ABAQUS (www.abaqus.com) will be used to obtain the equilibrium stress and strain fields. The crack faces are traction free, while symmetric conditions are used directly ahead of the crack. The loading of the CT specimen is controlled by prescribing the load-line displacement. Assuming a small-strain setting and imposing plane strain conditions, the equilibrium fields are calculated after each increment of displacement. The two isotropic materials are specified as either linear elastic or elastic-plastic using constitutive relations as formulated in ABAQUS. Linear elastic behavior is specified by prescribing the Young's modulus E and Poisson's ratio ν. For elastic-plastic materials isotropic incremental plasticity was chosen and elastic-plastic properties are specified by the yield stress σ_Y and the hardening coefficient N in addition to the elastic parameters E and ν. However, we note that for calculating C_{inh} using (3.16) ϕ was taken to be the total strain energy density and $u_{i,j}$ were gradients of the total displacement. Since load-line displacement is proportional we are effectively treating the elastic-plastic material as if it were nonlinear elastic.

Standard special elements are used at the crack tip to appropriately model the singular crack tip stresses for elastic, ideal elastic-plastic and elastic-plastic cases. The values of the J-integral in the far-field J_{far} and at the crack tip J_{tip} are evaluated using the standard J-integral evaluation procedure of ABAQUS. The post-processor provides the nodal values of $(\hat{\mathbf{e}} \cdot \mathbf{f}_\Sigma)$ (3.16) and the material inhomogeneity term C_{inh} (3.13). In order to have sufficient accuracy in evaluating $\mathbf{f}_\Sigma$, several element types and mesh sizes were examined. The optimum element was a higher order two-dimensional eight-node element and it was sufficient to take a minimum mesh size of 0.05 mm.

We now determine the crack tip shielding/anti-shielding due to inhomogeneity in elastic modulus, yield stress and hardening coefficient at a sharp bimaterial interface (so $\mathbf{f} = 0$, but $\mathbf{f}_\Sigma \cdot \mathbf{e} \neq 0$). For ease in reading, we refer to the component of the configurational interface force in the direction of crack growth, $\mathbf{f}_\Sigma \cdot \mathbf{e}$, as the '$C_{\text{inh}}$ density'. Throughout the paper, elastic moduli are specified in GPa, while yield stress is in MPa. Subscript 1 corresponds to the material on the left of the interface in Figure 2, while subscript 2 corresponds to the right and the crack is always in the material on the left. For all cases, the two materials will have the same Poisson's ratio $\nu = 0.3$.

4.1. Elastic bimaterial

The distribution of the C_{inh} density is shown for a stiff/compliant transition ($E_1/E_2 = 210/70$) in Figure 3a and for a compliant/stiff transition ($E_1/E_2 = 70/210$) in Figure 3b. In general, the magnitude of $\mathbf{f}_\Sigma \cdot \hat{\mathbf{e}}$ increases with increasing J_{far}. At a fixed value of J_{far}, it first increases slightly and then decays rapidly with increasing distance from the crack plane for the stiff/compliant case (Figure 3a); for the compliant/stiff case there is no observable increase, instead the magnitude of the C_{inh} density rapidly decays with increasing distance. Also $\mathbf{f}_\Sigma \cdot \hat{\mathbf{e}}$ is slightly larger when the crack is in the stiffer material than when it is in the more compliant material. The integration of the C_{inh} density along the whole interface yields a corresponding material inhomogeneity term C_{inh}, which scales linearly with the applied crack driving force J_{far} (see inset graphs in Figure 3) for both the stiff/compliant and compliant/stiff transitions. The stiff/compliant transition results in anti-shielding ($C_{\text{inh}} > 0$), and according to Equation (3.14), the

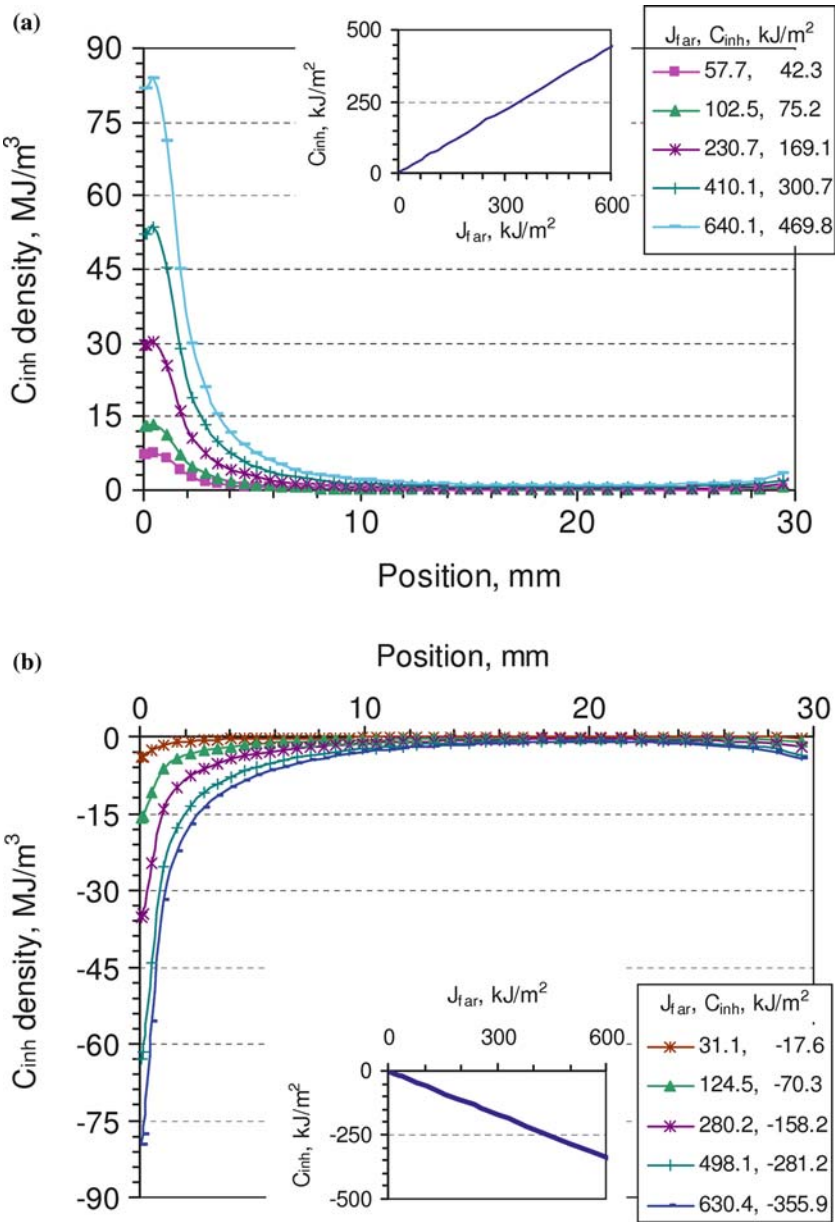

Figure 3. Elastic composite with mismatch in Young's modulus: the C_{inh} density, $\mathbf{f}_\Sigma \cdot \hat{\mathbf{e}}$, at positions along the bimaterial interface for (a) stiff/compliant case ($E_1/E_2 = 210/70$) and (b) compliant/stiff case ($E_1/E_2 = 210/70$). Corresponding C_{inh} versus J_{far} graphs are shown inset.

effective crack driving force is 73% larger than the far field value, i.e. $J_{\text{tip}} = 1.73 J_{\text{far}}$. The compliant/stiff transition results in shielding ($C_{\text{inh}} < 0$), and $J_{\text{tip}} = 0.44 J_{\text{far}}$.

To understand these trends, we obtain an estimate for $\mathbf{f}_\Sigma \cdot \hat{\mathbf{e}}$ based on Equations (3.8, B6). For an interface perpendicular to the crack plane, strain compatibility (3.8) requires that

$$[[u_{2,2}]] = [[u_{1,2}]] = 0$$

under plane strain conditions $\epsilon_{33}=\epsilon_{23}=\epsilon_{13}=0$ (crack and interface normal lie along the x_1 direction). So the only strain components that can have a jump at the interface are ϵ_{11} and ϵ_{12}. There are no simple ways to estimate these jumps. So in order to obtain an analytical estimate, we assume that these two components are continuous as well. The strain energy density can be written as $\phi=E\psi(\nu,\epsilon)$ (e.g. see pg. 246 of Timoshenko, 1959). For a constant homogeneous Poisson's ratio, Equation (B6) now becomes

$$\mathbf{f}_\Sigma\cdot\hat{\mathbf{e}}=-[[E]]\psi(\nu,\epsilon_{ij})=(E_1-E_2)\psi(\nu,\epsilon_{ij}). \tag{4.1}$$

The strain energy term $\psi\geqslant 0$. So, when $E_2>E_1$, $(\mathbf{f}_\Sigma\cdot\hat{\mathbf{e}})\leqslant 0$ and this inhibits crack growth towards the interface, whereas when $E_2<E_1$, $(\mathbf{f}_\Sigma\cdot\hat{\mathbf{e}})\geqslant 0$ and this assists crack growth towards the interface. If the sharp interface is instead treated as a graded interlayer, the sum over the interface width of $\mathbf{f}\cdot\hat{\mathbf{e}}$ is exactly the same as (4.1) (Simha et al., 2003).

Next, we estimate the strain at the interface by using the average value of the elastic moduli $\langle E\rangle$ and the usual plane strain LEFM crack tip stresses. Then, the configurational interface force component at a point at a distance y from the crack plane can be obtained from (4.1) as (Simha et al., 2003)

$$\mathbf{f}_\Sigma\cdot\hat{\mathbf{e}}=\frac{E_1-E_2}{E_1+E_2}\frac{J_{\text{far}}}{4\pi(1-\nu)L}\left[\frac{3-4\nu}{s}+\frac{(2-4\nu)}{s^2}-\frac{1}{s^3}\right], \tag{4.2}$$

where the non-dimensional radius $s=\sqrt{1+(y/L)^2}$. So the configurational interface force scales linearly with the applied crack driving force J_{far} (or K^2) and with the Dundurs parameter $(E_1-E_2)/(E_1+E_2)$ (Dundurs, 1969). In general, the plane isotropic elastic equilibrium problem for bimaterial composites depends on two parameters (Bogy, 1968, 1971), but the two parameters are identical when the Poisson's ratio is homogeneous, so it is appropriate that $\mathbf{f}_\Sigma\cdot\hat{\mathbf{e}}$ depends on this parameter. Also, since $(E_1-E_2)/(E_1+E_2)=(E_1/E_2-1)/(E_1/E_2+1)$, only the ratio of the elastic moduli are important and not the individual values. At the crack plane, $y=0$ so $s=1$ and

$$\mathbf{f}_\Sigma\cdot\hat{\mathbf{e}}=\frac{E_1-E_2}{E_1+E_2}\frac{(1-2\nu)J_{\text{far}}}{\pi(1-\nu)L}.$$

From this finite value, the interface force can initially increase with the distance from the crack plane, but eventually the $(1/s^3)$ term will dominate and then the interface force will decay to zero (explains trends in Figure 3a).

The analytical estimate (4.2) ignored jumps in strains ϵ_{11} and ϵ_{12} and used the homogeneous LEFM crack-tip stresses. Nevertheless, it correctly captures the primary dependences, i.e. the C_{inh} density scales with the Dundur's parameter and with the applied crack driving force, but is inversely proportional to the distance between the crack tip and the interface. The main deficiency is that the analytical estimates predicts the same magnitude when the crack is in either the stiffer or the more compliant material; in contrast, the numerical results show that the C_{inh} density is larger when the crack is in the stiffer material. Since the analytical estimate shows that the material interface force decays at large values of y, we can use the numerical results to suggest a length scale for this. In Figure 3 the material interface force has decayed to about 1% of its maximum value at $y=14.5\,\text{mm}$; since, the crack length is $a=29\,\text{mm}$, we can say that the material interface force can be neglected for $y\geqslant a/2$.

4.2. Elastic-plastic bimaterial

In the example considered here (Figure 2), there is no inhomogeneity in the bulk and the entire contribution to the crack tip shielding or anti-shielding is at the bimaterial interface. As mentioned before, we treat the elastic-plastic material as non-linear elastic to calculate the material inhomogeneity term, C_{inh}, and the component of the configurational interface force, C_{inh} density.

4.2.1. *Inhomogeneous elastic modulus*

Ignoring hardening ($N = 0$) and setting the yield stress $\sigma_{\text{Y}} = 500\,\text{MPa}$ and Poisson's ratio ν=0.3 for both materials, the C_{inh} density, $\mathbf{f}_{\Sigma} \cdot \hat{\mathbf{e}}$, is shown in Figure 4a for the stiff/compliant case ($E_1/E_2 = 70/210$) and in Figure 4b for the compliant/stiff case ($E_1/E_2 = 210/70$). First, consider the stiff/compliant case. At small values of the applied crack driving force (e.g. $J_{\text{far}} = 9.9\,\text{KJ/m}^2$), the elastic-plastic graph resembles the trends for the linear elastic case (cf. Figure 3a). However, for larger J_{far} there is a qualitative change in Figure 4a; $\mathbf{f}_{\Sigma} \cdot \hat{\mathbf{e}}$ has a maximum value at the crack plane and there is a drastic change in slope at values of $\approx 1.25\,\text{MJ/m}^3$. This kink appears at a certain distance from the crack plane where the plastic zone intersects with the interface; with increasing J_{far}, the plastic zone broadens and the kink moves to larger y values. In contrast, there is no significant qualitative differences between the elastic-plastic and linear elastic cases for the compliant/stiff transitions (cf. Figures 3b and 4b). More important is the quantitative differences between the elastic-plastic and linear elastic cases. For larger values of J_{far} ($> \approx 30\,\text{KJ/m}^2$) the C_{inh} density is stronger for the elastic case than for the elastic-plastic case. It increases linearly with J_{far} for the linear elastic case, whereas it saturates for the elastic-plastic case (negligible change for $J_{\text{far}} > 250\,\text{KJ/m}^2$ in Figure 4). Also, when the crack is in the stiffer material, the interface force is stronger and saturates at a higher value of J_{far}. These features are also reflected in the material inhomogeneity term C_{inh}, which increases sigmoidally with J_{far} initially, but saturates at higher values (see inset graphs in Figure 4). A case study of the dependency of the material inhomogeneity term for elastically inhomogeneous materials is presented in Kolednik et al. (2005).

4.2.2. *Inhomogeneous yield stress*

Fixing the elastic modulus at $E = 210\,\text{GPa}$, the Poisson's ratio at $\nu = 0.3$ and the hardening coefficient at $N = 0$ for both materials, the C_{inh} density ($\mathbf{f}_{\Sigma} \cdot \hat{\mathbf{e}}$) is obtained. The trends for the hard/soft case with $\sigma_{\text{Y1}}/\sigma_{\text{Y2}} = 900/300$ (Figure 5a) and for the soft/hard case with $\sigma_{\text{Y1}}/\sigma_{\text{Y2}} = 300/900$ (Figure 5b) are considerably different. For the hard/soft case, the C_{inh} density is stronger and primarily localized to a small region adjacent to the crack plane ($y \leqslant 2.5\,\text{mm}$ in Figure 4a); in contrast, it extends over a larger region of the interface for the soft/hard case, but it's magnitude is considerably smaller. For instance, the maximum magnitude of the interface force component is only $5.5\,\text{MJ/m}^3$ at $J_{\text{far}} \approx 175\,\text{KJ/m}^2$ for the soft/hard transition (Figure 5b), while it is about $70\,\text{MJ/m}^3$ for the corresponding hard/soft case (Figure 5a). By examining the distribution of the equivalent plastic strain (plots not shown), we find that the region with large C_{inh} density coincides exactly with the extent of the plastic zone along the interface. Also notice that the C_{inh} density is negligible until the applied crack driving force reaches a threshold value. The existence of a threshold J_{far} value

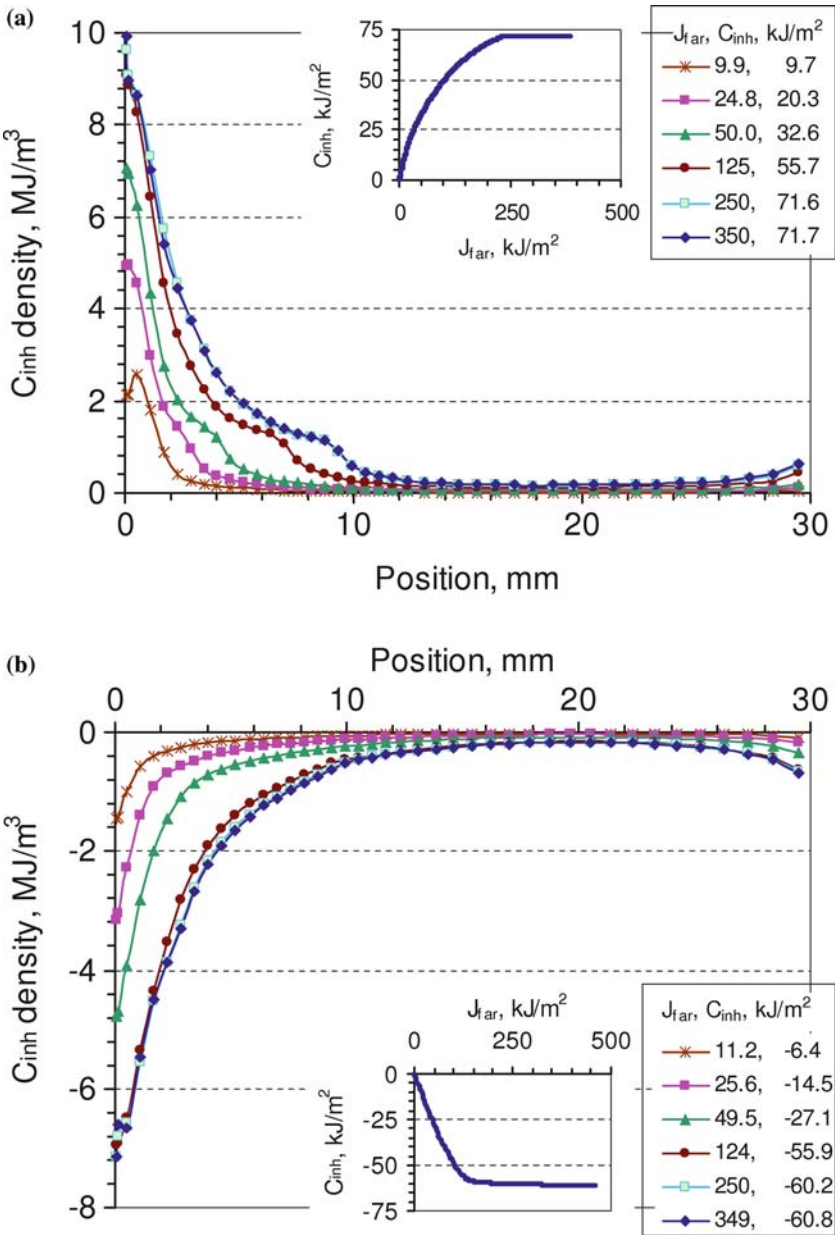

Figure 4. Elastic-plastic composite with mismatch in Young's modulus: $\mathbf{f}_\Sigma \cdot \hat{\mathbf{e}}$ at points along the bi-material interface for (a) stiff/compliant case ($E_1/E_2 = 210/70$) and (b) compliant/stiff case ($E_1/E_2 = 210/70$). Corresponding C_{inh} versus J_{far} graphs are shown inset.

is also reflected in the inhomogeneity term C_{inh}, and for J_{far} larger than this critical value C_{inh} increases almost linearly with J_{far} (inset graphs in Figure 5).

To understand the trends in Figure 5, we appeal to the analytical model of Kolednik (2000), who estimates the inhomogeneity effect due to yield stress mismatch at a sharp interface by assuming small-scale yielding, ignoring misfit strains and using circular plastic zones (which intersect the interface). In homogeneous materials

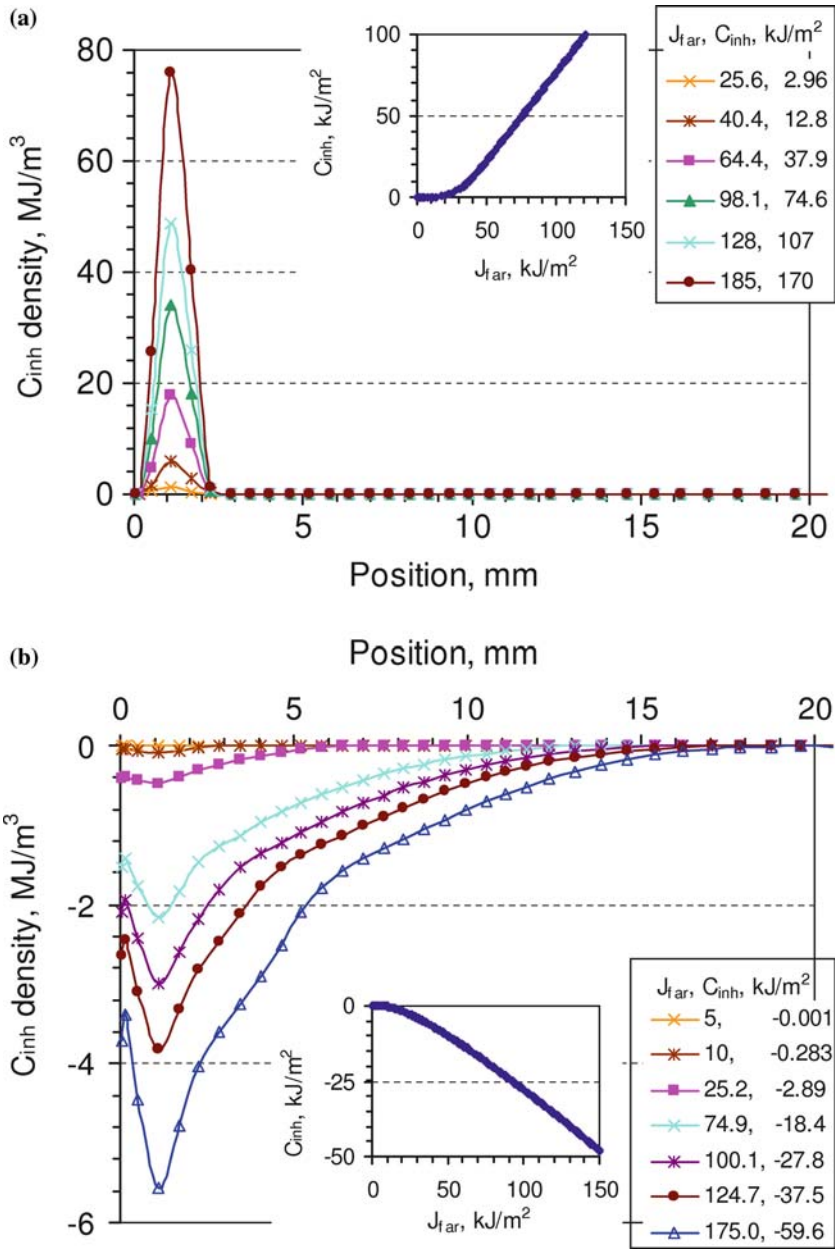

Figure 5. Elastic-plastic composite with mismatch in yield stress: $\mathbf{f}_\Sigma \cdot \hat{\mathbf{e}}$ at points along the bimaterial interface for (a) hard/soft case ($\sigma_{Y1}/\sigma_{Y2} = 900/300$) and (b) soft/hard case ($\sigma_{Y1}/\sigma_{Y2} = 300/900$). Corresponding C_{inh} versus J_{far} graphs are shown inset.

the radius of the plastic zone scales as $J_{far} E \sigma_Y^{-2}$. Adopting circular plastic zones, we can see that noticeable plasticity occurs at the interface, only if the radius of the plastic zone of the softer material reaches the interface. This immediately shows that a threshold value of J_{far} is necessary for the plastic zone to reach the interface; below that threshold, $\mathbf{f}_\Sigma \cdot \hat{\mathbf{e}}$ and, consequently, C_{inh} are negligible (Figure 5). A second result of Kolednik (2000) is that C_{inh} is directly proportional to the applied crack driving

force J_{far} and a function f_o that depends on the ratio of the plastic zone sizes in the materials to the left and right of the interface. As J_{far} increases beyond the threshold value, the plastic zone is completely developed. Then, the ratio of the plastic zone sizes is fixed, which fixes the function f_o; hence C_{inh} only has a linear dependence on J_{far} (Figure 5a and 5b).

5. Discussion and conclusions

This paper develops a configurational forces model to study effects of both smooth and discontinuous inhomogeneities on the crack driving force. The theoretical derivation shows that the configurational interface force $\mathbf{f}_\Sigma$ is equal to the jump in the normal component of the Eshelby tensor (3.2) and the configurational body force $\mathbf{f}$ is equal to the negative of the Lagrangian (explicit) gradient of the stored energy density (3.3); material is assumed to be hyperelastic only for obtaining the body force (3.3). The crack tip shielding/anti-shielding due to inhomogeneities is quantified by the material inhomogeneity term C_{inh}, which is obtained by integrating the configurational body force over the cracked body and the configurational interface force over the interface and then taking the component along the crack growth direction (3.4) or (3.5). Simplified expressions for $\mathbf{f}$, $\mathbf{f}_\Sigma$ and C_{inh} for linear elastic composites are given in Appendix B. The configurational forces as well as the material inhomogeneity term are evaluated by post-processing following a standard finite element stress analysis for a CT specimen. Cases considered include linear elastic with mismatch in elastic modulus (Figure 3) and elastic-plastic with mismatch in elastic modulus (Figure 4) or yield stress (Figure 5); deformational plasticity or proportional loading is assumed for the elastic-plastic case.

An extensive review of papers studying inhomogeneity effects on cracks has been given in Simha et al. (2003), so only papers dealing explicitly with sharp interfaces will now be discussed. Several papers consider interface cracks or use a K-field formulation that restricts their validity to linear elastic materials. For instance, Smelser and Gurtin (1977) consider cracks that lie on an interface between isotropic materials, then the material inhomogeneity has no contribution as $\hat{\mathbf{e}} \cdot \hat{\mathbf{n}} = 0$. Muju (2000) explicitly examines effects of bimaterial interfaces on cracks, but the K-field approach restricts the analysis to linear elastic materials. The J-integral approach has been extended for situations where a phase boundary is present in the vicinity of a crack by Miyamoto and Kikuchi (1980) and Weichert and Schulz (1993) who show that $J_{tip} = J_{far} - J_{int}$ where J_{int} is the J-integral taken over a contour that surrounds the phase boundary. It can be shown that $J_{int} \to -C_{inh}$ when the contour surrounding the phase boundary collapses onto the phase boundary. Weichert and Schulz (1993) examine a circular inclusion in front of the crack in a two-dimensional plane strain setting; the elastic modulus of the inclusion is 40% of the rest of the body and this inclusion changes the crack tip driving force by about 30%. Kikuchi amd Miyamoto (1984) study cracks lying on or touching grain boundaries; it is unclear how the contributions of J_{int} and J_{tip} are separated, nevertheless results show that inhomogeneities due to mis-orientation in elastic polycrystals as well as in the (isotropic) Young's modulus due to a second phase inclusion can have a significant effect on the crack driving force.

Although the total shielding/anti-shielding due to inhomogeneities is evaluated using C_{inh}, the configurational forces provide additional insights. For instance, it is useful to know that the C_{inh} density has a pronounced maximum either at or close to the crack plane for elastic modulus inhomogeneity and decays rapidly with increasing distance from the crack plane (Figures 3 and 4). It can be deduced from Figure 3 that an elastic particle of the size of 4 mm will have a similar effect as the whole bimaterial interface (spanning 60 mm in Figure 2) on a crack at a distance of $L = 0.6$ mm from the interface; the maximum is even more concentrated for smaller values of L, which suggests that small elastic particles have the potential for considerable shielding or anti-shielding. In case of yield stress inhomogeneity, a rather small soft particle may have a large effect on the effective crack driving force (Figure 5a), whereas a small hard particle will have a much smaller effect (Figure 5b).

For homogeneous materials, $\mathbf{f} = 0$ (and $\mathbf{f}_\Sigma = 0$). Nevertheless, the configurational body force has uses for numerical calculations. Braun (1997) has shown that numerical errors can lead to non-zero values of the configurational body force, even for convergent equilibrium stress (and strain) solutions. Consequently, $\mathbf{f}$ can be used as an error indicator in homogeneous stress analysis problems (Mueller and Maugin, 2002, Steinmann et al., 2001). Based on this, Denzer et al. (2003) and Mueller et al. (2004) develop adaptive meshing techniques to improve the accuracy of the stress analysis and J_{tip} evaluation. For inhomogeneous problems, one can first take constant material properties and use these methods to improve numerical accuracy, and then the same mesh can be used with inhomogeneous properties.

The material inhomogeneity term C_{inh}, and hence shielding or anti-shielding, scales linearly with applied driving force when there is mismatch in elastic modulus, so it will influence both the initiation and growth of fatigue cracks as well as final failure by unstable propagation. In contrast, inhomogeneity in yield stress will have a much smaller effect on fatigue crack initiation, although once the driving force value exceeds a threshold level it can significantly influence the growth of fatigue cracks. A second way to interpret the results is for high cycle fatigue versus low cycle fatigue. Elastic modulus inhomogeneity will influence both high and low cycle fatigue, whereas yield stress inhomogeneity will have a stronger influence on low cycle fatigue. Finally, the results obtained here suggest ways for tailoring materials to obtain desired fracture properties. For instance, if the goal is to design a sharp interface that has a negligible influence on the crack growth, one could choose values $E_1 > E_2$ (stiff to compliant), but with $\sigma_1 < \sigma_2$ (soft/hard). By examining the C_{inh} values in Figures 3 and 5, we suggest that $E_1/E_2 = (210\,\text{GPa})/(70\,\text{GPa})$ and $\sigma_{o1}/\sigma_{o2} = (200\,\text{MPa})/(500\,\text{MPa})$ may reduce $|C_{\text{inh}}|$ to about 5% of the applied driving force.

Acknowledgements

The authors would like to thank Prof. Steinmann for insightful discussions, the reviewers for useful comments and the Materials Center Leoben for funding (project numbers SP7 and SP14). Partial funding from the Christian Doppler Laboratorium Funktionsorientiertes Werkstoff-Design is also acknowledged. JP acknowledges the partial funding by the Österreichischer Austauschdienst (ÖAD) and the Slovenian Ministry of Education, Science and Sport (bilateral project Sl-A 12/0405).

Appendix A: modified divergence theorem

Certain bulk fields can be singular at the crack tip, hence we calculate the area integral over a region $\mathcal{D}$ that contains the crack tip as

$$\int_{\mathcal{D}} \mathbf{b}\,\mathrm{d}A := \lim_{r\to 0} \int_{\mathcal{D}\setminus\mathcal{B}_r} \mathbf{b}\,\mathrm{d}A$$

where $\mathcal{B}_r$ is a disk of radius r centered at the crack tip. For a region $\mathcal{D}$ that contains the crack tip and intersects with the bimaterial interface Σ, we use the above definition for area integral and apply the usual divergence theorem; then one can obtain (Simha and Bhattacharya, 1998)

$$\int_{\mathcal{D}} \nabla\cdot\mathbf{b}\,\mathrm{d}A = \int_{\partial\mathcal{D}} \mathbf{b}\cdot\hat{\mathbf{m}}\,\mathrm{d}l - \lim_{r\to 0}\int_{\partial\mathcal{B}_r} \mathbf{b}\cdot\hat{\mathbf{m}}\,\mathrm{d}l - \int_{C\cap\mathcal{D}} [[\mathbf{b}]]\cdot\hat{\mathbf{p}}\,\mathrm{d}l - \int_{\Sigma\cap\mathcal{D}} [[\mathbf{b}]]\cdot\hat{\mathbf{n}}\,\mathrm{d}l, \tag{A1}$$

where $C\cap\mathcal{D}$ denotes the part of the crack and $\Sigma\cap\mathcal{D}$ denotes the part of the interface that lie in the region $\mathcal{D}$. Then by taking $\mathbf{b}=\mathbf{B}^{\mathrm{T}}\mathbf{a}$ where $\mathbf{a}$ is some constant vector, we get

$$\int_{\mathcal{D}} \nabla\cdot\mathbf{B}\,\mathrm{d}A = \int_{\partial\mathcal{D}} \mathbf{B}\hat{\mathbf{m}}\,\mathrm{d}l - \lim_{r\to 0}\int_{\partial\mathcal{B}_r} \mathbf{B}\hat{\mathbf{m}}\,\mathrm{d}l - \int_{C\cap\mathcal{D}} [[\mathbf{B}]]\hat{\mathbf{p}}\,\mathrm{d}l - \int_{\Sigma\cap\mathcal{D}} [[\mathbf{B}]]\hat{\mathbf{n}}\,\mathrm{d}l\,. \tag{A2}$$

Appendix B: linear elastic expressions for $\mathbf{f}$, $\mathbf{f}_\Sigma$, and $\mathbf{C}_{\mathrm{inh}}$

For linear elastic materials the strain energy density is

$$\phi = \frac{1}{2}\mathbf{E}\boldsymbol{\epsilon}\cdot\boldsymbol{\epsilon} = \frac{1}{2}E_{ijkl}\epsilon_{ij}\epsilon_{kl}, \tag{B1}$$

where $\mathbf{E}$ is the fourth-order tensor of elastic moduli and the second expression above is written in Cartesian components. In the case of smoothly varying material properties $\mathbf{E}=\mathbf{E}(\mathbf{x})$ and the configurational body force is obtained from gradient of the stored energy in (3.10) as

$$\mathbf{f} = -\nabla_{\mathbf{x}}\phi(\boldsymbol{\epsilon},\mathbf{x}) = -\frac{1}{2}\frac{\mathrm{d}\mathbf{E}}{\mathrm{d}\mathbf{x}}\boldsymbol{\epsilon}\cdot\boldsymbol{\epsilon} \quad \text{or} \quad f_{\mathrm{p}} = -\frac{1}{2}\frac{\mathrm{d}E_{ijkl}}{\mathrm{d}x_p}\epsilon_{ij}\epsilon_{kl} \tag{B2}$$

Thus, the calculation of f_{p} is similar to evaluating the stored energy density except the gradient of the moduli are used in place of the elastic moduli.

The following identities will be useful for obtaining the configurational interface force at sharp interfaces

$$[[ab]] = \langle a\rangle[[b]] + [[a]]\langle b\rangle, \tag{B3}$$

$$\langle a\rangle\langle b\rangle - \langle ab\rangle = -\frac{1}{4}[[a]][[b]], \tag{B4}$$

$$\langle a\rangle^2 - \frac{[[a]]^2}{4} = a^+a^-. \tag{B5}$$

Using the strain energy density (B1), the term

$$[[\phi]] - \langle \boldsymbol{\sigma} \rangle \cdot [[\boldsymbol{\epsilon}]] = \frac{1}{2}[[\mathbf{E}\boldsymbol{\epsilon} \cdot \boldsymbol{\epsilon}]] - \langle \boldsymbol{\sigma} \rangle \cdot [[\boldsymbol{\epsilon}]] = \frac{1}{2}[[\boldsymbol{\sigma} \cdot \boldsymbol{\epsilon}]] - \langle \boldsymbol{\sigma} \rangle \cdot [[\boldsymbol{\epsilon}]]$$
$$= \frac{1}{2}\left([[\boldsymbol{\sigma}]] \cdot \langle \boldsymbol{\epsilon} \rangle - \langle \boldsymbol{\sigma} \rangle \cdot [[\boldsymbol{\epsilon}]]\right) = \frac{1}{2}\left([[\mathbf{E}\boldsymbol{\epsilon}]] \cdot \langle \boldsymbol{\epsilon} \rangle - \langle \mathbf{E}\boldsymbol{\epsilon} \rangle \cdot [[\boldsymbol{\epsilon}]]\right),$$

where we have use the stress-strain relation $\boldsymbol{\sigma} = \mathbf{E}\boldsymbol{\epsilon}$ and the identity (B3); note that the stress still has to satisfy the traction continuity condition (3.8) at the sharp interface. Next, using (B3) again, we get $[[\mathbf{E}\boldsymbol{\epsilon}]] \cdot \langle \boldsymbol{\epsilon} \rangle = [[\mathbf{E}]]\langle \boldsymbol{\epsilon} \rangle \cdot \langle \boldsymbol{\epsilon} \rangle + \langle \mathbf{E} \rangle [[\boldsymbol{\epsilon}]] \cdot \langle \boldsymbol{\epsilon} \rangle$. As the elastic moduli are symmetric, we get

$$\left([[\mathbf{E}\boldsymbol{\epsilon}]] \cdot \langle \boldsymbol{\epsilon} \rangle - \langle \mathbf{E}\boldsymbol{\epsilon} \rangle \cdot [[\boldsymbol{\epsilon}]]\right) = [[\mathbf{E}]]\langle \boldsymbol{\epsilon} \rangle \cdot \langle \boldsymbol{\epsilon} \rangle + \left(\langle \mathbf{E} \rangle \langle \boldsymbol{\epsilon} \rangle - \langle \mathbf{E}\boldsymbol{\epsilon} \rangle\right) \cdot [[\boldsymbol{\epsilon}]].$$

Then, using identities (B4) and (B5), we rewrite the jump as

$$[[\phi]] - \langle \boldsymbol{\sigma} \rangle \cdot [[\boldsymbol{\epsilon}]] = \frac{1}{2}[[\mathbf{E}]]\left(\langle \boldsymbol{\epsilon} \rangle \cdot \langle \boldsymbol{\epsilon} \rangle - \frac{[[\boldsymbol{\epsilon}]] \cdot [[\boldsymbol{\epsilon}]]}{4}\right) = \frac{1}{2}[[\mathbf{E}]]\boldsymbol{\epsilon}^+ \cdot \boldsymbol{\epsilon}^-.$$

Consequently, the force component (3.12) can be written as

$$\hat{\mathbf{e}} \cdot \mathbf{f}_\Sigma = -\frac{1}{2}\left([[\mathbf{E}]]\boldsymbol{\epsilon}^+ \cdot \boldsymbol{\epsilon}^-\right)(\hat{\mathbf{e}} \cdot \hat{\mathbf{n}}) = -\frac{1}{2}\left([[E_{ijkl}]]\epsilon_{ij}^+ \epsilon_{kl}^-\right)(e_\mathrm{p} n_\mathrm{p}), \tag{B6}$$

where e_p denotes the Cartesian components of crack growth direction vector $\hat{\mathbf{e}}$ and the strain values on the right side of the interface are $\boldsymbol{\epsilon}^+$, while $\boldsymbol{\epsilon}^-$ are on the left. Note that calculating $\hat{\mathbf{e}} \cdot \mathbf{f}_\Sigma$ is similar to evaluating the strain energy density, except that the jump in moduli are used in place of the elastic moduli.

Finally, the material inhomogeneity term (3.13) for elastic composites is

$$C_\mathrm{inh} = -\int_\mathcal{B}\left(\frac{\mathbf{e}}{2} \cdot \frac{\mathrm{d}\mathbf{E}}{\mathrm{d}\mathbf{x}}\right)\boldsymbol{\epsilon} \cdot \boldsymbol{\epsilon}\,\mathrm{d}A - \frac{1}{2}\int_\Sigma \left([[\mathbf{E}]]\boldsymbol{\epsilon}^+ \cdot \boldsymbol{\epsilon}^-\right)(\hat{\mathbf{e}} \cdot \hat{\mathbf{n}})\mathrm{d}l$$
$$= -\int_\mathcal{B}\left(\frac{e_p}{2}\frac{\mathrm{d}E_{ijkl}}{\mathrm{d}x_p}\right)\epsilon_{ij}\epsilon_{kl}\,\mathrm{d}A - \frac{1}{2}\int_\Sigma \left([[E_{ijkl}]]\epsilon_{ij}^+ \epsilon_{kl}^-\right)(e_\mathrm{p} n_\mathrm{p})\mathrm{d}l. \tag{B7}$$

References

Abeyaratne, R. and Knowles, J.K. (1990). On the driving traction acting on a surface of strain discontinuity in a continuum. *J. Mech. Phys. Solids* **38**, 345–360.

Bogy, D.B. (1968). Edge-bonded dissimilar orthogonal elastic wedges under normal and shear loading. *ASME J. App. Mech.* **35**, 460–466.

Bogy, D.B. (1971). Two edge-bonded elastic wedges of different materials and wedge angles under surface tractions. *ASME Journal of Applied Mechanics* **38**, 377–386.

Braun, M. (1997). Configurational forces induced by finite-element discretization. *Proc. Estonian Acad. Sci. Phys. Math.* **46**, 24–31.

Denzer, R., Barth, F.J. and Steinmann, P. (2003). Studies in elastic fracture mechanics based on the material force method. *Int. J. Numer. Meth. Eng.* **58**, 1817–1835.

Dundurs, J. (1969). Edge-bonded dissimilar orthogonal elastic wedges. *ASME Journal of Applied Mechanics* **36**, 650–652.

Ericksen, J.L. (1977). Special topics in elastostatics. In: *Advances in Applied Mechanics* (edited by Yih, C.-S.), Vol. 17. Academic Press, New York, pp. 189–244.

Eshelby, J.D. (1970). Energy relations and the energy-momentum tensor in continuum mechanics. In: *Inelastic Behavior of Solids* (edited by Kanninen, M. et al.), McGraw Hill, New York, 77–115.

Gurtin, M.E. (1995). The nature of configurational forces. *Arch. Rational Mech. Anal.* **131**, 67–100.

Gurtin, M.E. (2000). *Configurational Forces as Basic Concepts of Continuum Physics*. Springer, New York.

Gurtin, M.E. and Podio-Guidugli, P. (1996). Configurational forces and the basic laws for crack propagation. *Journal of the Mechanics Physics of Solids* **44**(6), 905–927.

Kienzler, R. and Herrmann, G. (2000). *Mechanics in Material Space*. Springer, Berlin.

Kikuchi, M. and Miyamoto, H. (1984). Application of the *J*-integral concept to microscopic fracture mechanics. In: *Mechanical Behavior of Materials IV, Proceedings of the Fourth International Conference* (edited by Carlsson, J. and Ohlson, N.G.), Vol. 2. Pergamon, Oxford, UK, 1077–1083.

Kolednik, O. (2000). The yield stress gradient effect in inhomogeneous materials. *Int. J. Solids Struct.* **37**, 781–808.

Kolednik, O., Predan, J., Shan, G.X., Simha, N.K. and Fischer, F.D. (2005). On the fracture behavior of inhomogeneous materials – a case study for elastically inhomogeneous bimaterials. *International Journal of Solids Structures* **42**, 605–620.

Maugin, G.A. (1993). *Material Inhomogenieties in Elasticity*. Chapman and Hall, London.

Maugin, G.A. (1995). Material forces: Concepts and applications. *ASME Appl. Mech. Rev.* **48**, 213–245.

Maugin, G.A. and Trimarco, C. (1992). Pseudo-momentum and material forces in nonlinear elasticity: Variational formulation and application to brittle fracture. *Acta Mech* **94**, 1–28.

Mueller, R., Gross, D. and Maugin, G.A. (2004). Use of material forces in adaptive finite element methods. *Comp. Mech.* **33**, 421–434.

Mueller, R., Kolling, S. and Gross, D. (2002). On configurational forces in the context of the finite element method. *Int. J. Numer. Meth. Eng.* **53**, 1557–1574.

Mueller, R. and Maugin, G.A. (2002). On material forces and finite element discretizations. *Comp. Mech.* **29**, 52–60.

Miyamoto, H. and Kikuchi, M. (1980). In: *Proceedings of the Second International Conference in Numerical Methods in Fracture Mechanics* (edited by Owen, D.R.J. and Luxmore, A.R.), PineRidge Press, Swansea, UK, 359–370.

Muju, S. (2000). Crack propagation in bimaterial multilayered periodically microcracking composite media. *Compos. Sci. Technol.* **60**, 2213–2221.

Pippan, R. and Flechsig, K. (2000). Fatigue crack propagation behavior in the vicinity of an interface between materials with different yield stresses. *Mat. Sci. Eng.* **A283**, 225–233.

Rice, J.R. (1968). Mathematical analysis in the Mechanics of Fracture, in *Fracture* (edited by Liebowitz, H.), Vol. II. Academic Press, 379–386.

Simha, N.K. (2000). Toughening by phase boundary propagation. *J. Elasticity* **59**, 195–211.

Simha, N. K. and Bhattacharya, K. (1998). Kinetics of a phase boundary with edges and junctions. *Journal of the Mechanics and Physics of Solids* **46**, 2323–2359.

Simha, N.K., Fischer, F. D., Kolednik, O. and Chen, C. R. (2003). Inhomogeneity effects on the crack driving force in elastic and elastic-plastic materials. *Journal of the Mechanics and Physics of Solids* **51**, 209–240.

Steinmann, P. (2000). Application of material forces to hyperelastostatic fracture mechanics. Part I: Continuum mechanical setting. *International Journal of Solids Structures* **37**, 7371–7391.

Steinmann, P., Ackermann, D. and Barth, F.J. (2001). Application of material forces to hyperelastostatic fracture mechanics. Part II: Computational Setting. *International Journal of Solids Structures* **38**, 5509–5526.

Smelser, R.E. and Gurtin, M.E. (1977). On the *J*-Integral for bi-material bodies. *Int. J. Fracture* **13**, 382–384.

Suresh, S., Sugimura, Y. and Tschegg, E. (1992). The growth of a fatigue crack approaching a perpendicularly-oriented, bimaterial interface. *Scripta Metall.* **27**, 1189–1194.

Timoshenko, S. (1959). *Theory of Elasticity*. McGraw-Hill, New York.

Truskinovsky, L. (1982). Equilibrium interphase boundaries. *Dokl. Akad. Nauk. SSSR.* **275**, 306–310.

Weichert, D. and Schulz, M. (1993). *J*-integral concept for multi-phase materials. *Comput. Mat. Sci.* **1**, 241–248.